Inorg. Chem. **2005**, *44*, 6609–6622

Structural, Optical, and Photophysical Properties of Nickel(II) Alkylthioporphyrins: Insights from Experimental and DFT/TDDFT Studies

Angela Rosa,*,§ Giampaolo Ricciardi,*,§ Evert Jan Baerends,‡ Mikhail Zimin,⊥ Michael A. J. Rodgers,*,⊥ Shingo Matsumoto,† and Noboru Ono†

Dipartimento di Chimica, Università della Basilicata, Via N. Sauro 85, 85100 Potenza, Italy, Afdeling Theoretische Chemie, Vrije Universiteit, De Boelelaan 1083, 1081 HV Amsterdam, The Netherlands, Center for Photochemical Sciences and Department of Chemistry, Bowling Green State University, Bowling Green, Ohio 43403, Department of Chemistry, Faculty of Science, Ehime University, Matsuyama 790 8577, Japan

Received May 24, 2005

The ground- and excited-state properties of a Ni(II) porphyrin bearing peripheral alkylthio group, NiOMTP (OMTP = 2,3,7,8,12,13,17,18-octakis methylthio porphyrinate) have been investigated by steady-state and time-resolved absorption spectrometry and DFT/TDDFT theoretical methods. Several conformations corresponding to different deformations of the porphyrin core and to different orientations of the alkylthio groups have been theoretically explored. The nearly degenerate, purely ruffled D_{2d} and hybrid (ruffled with a modest degree of saddling) D_2 conformations, both characterized by an up–down (*ud*) orientation of the vicinal methylthio groups are by far the preferred conformations in the "gas phase". In contrast to NiOEP, it is the orientation of the peripheral substituents rather than the type and degree of distortions of the porphyrin core that determines the stability of the NiOMTP conformers. The ground-state electronic absorption spectra of NiOMTP exhibit significant changes compared to its parent NiP and β-alkylated analogues, such as NiOEP, resulting in a considerable red shift of the B and the Q bands, intensification and broadening of the Q band, and additional weak absorptions in the region between the Q and B bands. These spectral changes can be understood in terms of the electronic effects of the methylthio groups with nonplanar distortions of the porphyrin ring playing a very minor role. Transient absorption measurements with sub-picosecond resolution performed in toluene and TDDFT calculations reveal that following photoexcitation, NiOMTP deactivates by the pathway $^1(\pi,\pi^*) \rightarrow {}^3(d_{z^2},d_{x^2-y^2}) \rightarrow$ ground state. The (d,d) state exhibits complex spectral evolution over ca. 8 ps, interpreted in terms of vibrational relaxation and cooling. The cold ligand-field excited state decays with a lifetime of 320 ps. At variance with the highly distorted nickel porphyrins but similar to the planar analogues, the (d,d) spectrum of NiOMTP has transient absorption bands immediately to the red of the bleaching of the ground-state Q and B bands.

Introduction

It has been well documented that the physical, chemical, and biological properties of porphyrins and metalloporphyrins can be fine-tuned or dramatically altered by introducing heteroatoms or heteroatom-based groups at the β, meso, or both positions of the macrocycle.[1−16] For instance, the introduction of more than four halogens at the β-pyrrole

* To whom correspondence should be addressed. E-mail: rosa@unibas.it (A.R.); rg010sci@unibas.it (G.R.); rodgers@bgnet.bgsu.edu (M.A.J.R.).
§ Università della Basilicata.
‡ Vrije Universiteit.
⊥ Bowling Green State University.
† Ehime University.

(1) Jaquinod, L. Heteroatom Porphyrins. In *The Porphyrin Handbook*; Kadish, K. M., Smith, K. M., Guilard, R., Eds.; Academic Press: San Diego, CA, 2000; Vol. I., p 201.
(2) Kalish, H.; Camp, J. E.; Stepien, M.; Latos-Grazynski, L.; Olmstead, M. M.; Balch, A. L. *Inorg. Chem.* **2002**, *41*, 989.
(3) Kalish, H.; Camp, J. E.; Stepien, M.; Latos-Grazynski, L.; Balch, A. L. *J. Am. Chem. Soc.* **2001**, *123*, 11719.
(4) Sibilia, S. A.; Czernuszewicz, R. S.; Crossley, M. J.; Spiro, T. G. *Inorg. Chem.* **1997**, *36*, 6450.
(5) Binstead, R. A.; Crossley, M. J.; Hush, N. S. *Inorg. Chem.* **1991**, *30*, 1259.

10.1021/ic050838t CCC: $30.25
Published on Web 08/24/2005

carbon results in the distortion of the macrocycle, large ground-state spectral and oxidation potential shifts,[10,11] enhanced optical limiting properties,[9] and improved catalytic activity.[14−16] Similarly, the introduction of aryloxy and alkoxyl substituents or arylamino and alkylamino groups at the periphery of the macrocycle has been shown to induce relevant changes in the physicochemical properties of porphyrins.[2−9] In marked contrast to the considerable number of synthetic porphyrins that have halogen, nitrogen, oxygen heteroatom substituents attached to the periphery of the porphyrin core, only a few porphyrins bearing sulfur-based substituents are known, namely H_2OMTP[17,18] and its manganese, zinc,[17] and nickel[18] derivatives. The use of alkylthioporphyrins as building blocks for supramolecular architectures constructed with the chalcogen−chalcogen atomic contacts usually seen in tetrathiafulvalene-based conductors has motivated most of the research work on this family of porphyrins. Actually, the Mn(III)OMTP derivative was shown to form the $[Mn^{III}OMTP]^+[TCNE]^{-\cdot}$ electron-transfer salt (ETS) with a 1D uniform structure that stabilizes ferrimagnetic coupling.[17]

The physicochemical properties of alkylthioporphyrins, which may be relevant to the design and synthesis of new materials based on this novel class of porphyrins, have never been investigated. For H_2OMTP only, ^{1}H NMR and UV−vis absorption and emission spectra have been reported and compared with the corresponding H_2OEP (OEP = octaethylporphyrin) and H_2OMOP (OMOP = octamethoxyporphyrin) data.[18]

The aim of this paper is to explore the impact of alkylthio substitution on the ground- and excited-state properties of metalloporphyrins. Among the different metalloalkylthioporphyrins, nickel(II) alkylthioporphyrins are specially suited for this purpose because of the availability of numerous experimental and theoretical studies on a large variety of Ni(II) porphyrins (see refs 19−31 and references therein).

We will focus here on the conformational, optical, and photophysical properties of NiOMTP, a complex that we were able to synthesize through a new methodology that combines an efficient synthetic route to the 3,4-bis(methylthio)pyrrole with the cyclotetramerization method of Ono et al.[32] and Sakata et al.[18]

Ni(II) porphyrins show a rich conformational behavior because the small ionic radius of 0.69 Å for nickel(II)[33] tends to pull the pyrrole rings inward and contract the core, resulting in a small deformation of porphyrins normally considered planar,[34] such as NiOEP.[21,25] As a matter of fact, planar Ni porphyrins are found in solution only when the peripheral substituents are hydrogen atoms (NiP)[24] or when the steric constraints imposed by the substituents make in-plane distortion preferable.[19] All other Ni porphyrins in solution are either nonplanar or a mixture of the nonplanar and planar forms, with nonplanar ones as the lowest-energy structures.[20,21]

In nickel alkylthioporphyrins, the steric conflicts of the peripheral substituents are expected to amplify the metal-induced distortion of the porphyrin core.[34] Furthermore, just as in NiOEP, different orientations of the alkylthio groups can generate several conformers.[25] In the absence of structural data, we have performed an accurate theoretical investigation of the ground-state energy surface of NiOMTP, using density functional theory (DFT) methods. In an attempt to assess the nonplanar distortion induced by the peripheral methylthio groups, the structure of the parent NiP has also been theoretically reinvestigated.

The amplification of the distortion of the porphyrin core induced by the alkylthio groups could be, in principle, the origin of the red shift of the Q and B bands observed in H_2OMTP[18] and in the presently investigated nickel(II) derivative (vide infra). Indeed, red shifting upon nonplanarity in NiOEP has been very recently demonstrated by Evans and Musselman through solid-state polarized UV−vis spectroscopy and ZINDO calculations.[23] In alkylthioporphyrins, however, the electronic effects of the conjugation between the diffuse sulfur lone pairs and the porphyrin π-system could also play a relevant role so that the observed changes in the

(6) Murashima, T.; Uchihara, Y.; Wakamori, N.; Uno, H.; Ogawa, T.; Ono, N. *Tetrahedron Lett.* **1996**, *37*, 3133.
(7) Gao, G.-Y.; Colvin, A. J.; Chen, Y.; Zhang, X. P. *Org. Lett.* **2003**, *5*, 3261.
(8) Merz, A.; Schropp, R.; Lex, J. *Angew. Chem., Int. Ed. Engl.* **1993**, *32*, 291.
(9) Su, W.; Cooper, T. M. *Chem. Mater.* **1998**, *10*, 1212.
(10) D'Souza, F.; Zandler, M. E.; Tagliatesta, P.; Ou, Z.; Shao, J.; van Caemelbecke, E.; Kadish, K. M. *Inorg. Chem.* **1998**, *37*, 4567.
(11) Spyroulias, G. A.; Despotopoulos, A. P.; Raptopoulou, C. P.; Terzis, A.; de Montauzon, D.; Poiblanc, R.; Coutsolelos, A. G. *Inorg. Chem.* **2002**, *41*, 4648.
(12) Woller, E. K.; DiMagno, S. G. *J. Org. Chem.* **1997**, *62*, 1588.
(13) Leroy, J.; Bondon, A.; Toupet, L.; Rolando, C. *Chem.—Eur. J.* **1997**, *3*, 1890.
(14) Ellis, P. E., Jr.; Lyons, J. E. *Catal. Lett.* **1989**, *3*, 389.
(15) Lyons, J. E.; Ellis, P. E., Jr. *Catal. Lett.* **1991**, *8*, 45.
(16) Chorghade, M. S.; Hill, D. R.; Lee, E. C.; Pariza, R. J.; Dolphin, D.; Hino, F.; Zhang, L.-Y. *Pure Appl. Chem.* **1996**, *68*, 753.
(17) Sugiura, K.; Ushiroda, K.; Johnson, M. T.; Miller, J. S.; Sakata, Y. *J. Mater. Chem.* **2000**, *10*, 2507.
(18) Sugiura, K.; Kumar, M. R.; Chandrashekar, T. K.; Sakata, Y. *Chem. Lett.* **1997**, 291.
(19) Shelnutt, J. A.; Medforth, C. J.; Berber, M. D.; Barkigia, K. M.; Smith, K. M. *J. Am. Chem. Soc.* **1991**, *113*, 4077.
(20) Anderson, K. K.; Hobbs, J. D.; Luo, L.; Stanley, K. D.; Quirke, J. M. E.; Shelnutt, J. A. *J. Am. Chem. Soc.* **1993**, *115*, 12346.
(21) Alden, R. G.; Crawford, B. A.; Doolen, R.; Ondrias, M. R.; Shelnutt, J. A. *J. Am. Chem. Soc.* **1989**, *111*, 2070.
(22) Retsek, J. L.; Drain, C. M.; Kirmaier, C.; Nurco, D. J.; Medforth, C. J.; Smith, K. M.; Sazanovich, I. V.; Chirvony, V. S.; Fajer, J.; Holten, D. *J. Am. Chem. Soc.* **2002**, *125*, 9787.
(23) Evans, J. S.; Musselman, R. L. *Inorg. Chem.* **2004**, *43*, 5613.
(24) Jentzen, W.; Turowska-Tyrk, I.; Scheidt, W. R.; Shelnutt, J. A. *Inorg. Chem.* **1996**, *35*, 3559.
(25) Stoll, L. K.; Zgierski, M. Z.; Kozlowski, P. M. *J. Phys. Chem. A* **2002**, *106*, 170.
(26) Kim, D.; Holten, D. *Chem. Phys. Lett.* **1983**, *98*, 584.
(27) Kim, D.; Kirmaier, C.; Holten, D. *Chem. Phys.* **1983**, *75*, 305.
(28) Drain, C. M.; Kirmaier, C.; Medforth, C. J.; Nurco, D. J.; Smith, K. M.; Holten, D. *J. Phys. Chem.* **1996**, *100*, 11984.
(29) Rosa, A.; Baerends, E. J. *Inorg. Chem.* **1993**, *32*, 5637.
(30) Rosa, A.; Ricciardi, G.; Baerends, E. J.; van Gisbergen, S. J. A. *J. Phys. Chem. A* **2001**, *105*, 3311.
(31) Drain, C. M.; Gentemann, S.; Roberts, J. A.; Nelson, N. Y.; Medforth, C. J.; Jia, S.; Simpson, M. C.; Smith, K. M.; Fajer, J.; Shelnutt, J. A.; Holten, D. *J. Am. Chem. Soc.* **1998**, *120*, 3871.
(32) Ono, N.; Kawamura, H.; Bougauchi, M.; Maruyama, K. *Tetrahedron* **1990**, *46*, 7483.
(33) Pauling, L. *The Nature of the Chemical Bond*, 3rd ed.; Cornell University Press: Ithaca, NY, 1960.
(34) Hoard, J. L. *Science* **1971**, *174*, 1295.

optical spectra may result from the interplay between electronic and structural (ultimately electronic) factors.

The effects, on the steady-state electronic absorption spectra, of introducing eight methylthio groups to the bare nickel porphyrin (NiP) have been quantified by time-dependent density functional theory (TDDFT) calculations of the excited states of NiOMTP and NiP. The interpretation of the spectral changes, such as the considerable bathochromic shift of the Q and B bands and the intensification of the Q-band observed in the solution absorption spectra of NiOMTP relative to NiP and NiOEP, has been based on a detailed analysis of the ground-state electronic structure.

For the photophysical behavior of nickel alkylthioporphyrins, the electronic and structural factors responsible for the changes in the ground-state absorption spectra are also likely to affect the excited-state relaxation dynamics. According to previous studies,[35,36] the nominally planar nickel porphyrins, such as NiTPP (TPP = *meso*-tetraphenylporphyrin) and NiOEP, in noncoordinating solvents, show rapid radiationless decay of the primarily excited $^1(\pi,\pi^*)$ state via the low-energy singlet, triplet, or both forms of the $(d_{z^2},d_{x^2-y^2})$ state. Ultrafast absorption measurements of NiTPP and NiOEP have revealed that a (d,d) state forms within <1 ps,[37−39] followed by deactivation to the ground state in 200−500 ps.[26,27,40−44]

The deactivation mechanism proposed for the nominally planar nickel porphyrins also holds for highly distorted Ni(II) porphyrins, such as NiDPP (DPP = dodecaphenylporphyrin).[28] However, whereas the (d,d) difference spectra for the planar compounds all have absorption bands indicating a red shift from the ground-state Soret and Q bands, the (d,d) difference spectra of the highly distorted nickel porphyrins have Soret and Q bands that are blue shifted from those of the ground state.[28] Whether the excited-state behavior of NiOMTP is more similar to that of the nominally planar nickel porphyrins or to that of the distorted ones is an important question to be addressed. To this end, we have performed ultrafast transient absorption spectroscopy experiments on NiOMTP, in a noncoordinating solvent (toluene) and interpreted the excited-state spectral and dynamic behavior with the help of DFT/TDDFT calculations of the lowest-excited states of the complex.

Experimental Section

Materials. Solvents for the reactions were freshly distilled over appropriate drying agents prior to use. Reactions that required oxygen-free conditions were carried out under an inert atmosphere of nitrogen in oven-dried glassware using standard Schlenk techniques. Solvents of spectroscopic or HPLC grade for spectroscopic experiments were purchased from Aldrich Chemical Co.

Instrumentation. Electronic absorption spectra were recorded in toluene using a Varian Cary 50 Bio single-beam spectrophotometer or a Varian Cary 500E double-beam spectrophotometer. ^{1}H and ^{13}C NMR spectra were recorded on a Varian INOVA 500 (499.5987 MHz for ^{1}H, 125.6242 MHz for ^{13}C) spectrometer at room temperature using TMS as the internal standard. The pump−probe instrument for ultrafast transient absorption measurements has been described previously.[45] The recent improvements to enhance signal-to-noise characteristics have been communicated elsewhere.[46] A Spectra-Physics Tsunami/Spitfire Ti/sapphire combination generated 800 nm pulses of nominally 100 fs in duration at a rate of 1 kHz**.** In the current experiments, the excitation wavelength of 400 nm was derived from the second harmonic of the Ti/sapphire fundamental and that, at 582 nm, was generated with an optical parametric amplifier (OPA 800, Spectra-Physics).

Synthesis of NiOMTP. The synthesis of NiOMTP involves four steps as described below.

***N*-tosyl-(1,3)-dithiolo[4,5-c]pyrrole-2-thione (1).** Compound **1** was prepared according to the literature method.[47]

3,4-Bis(methylthio)pyrrole (2). A solution of NaH (0.63 mg) in MeOH (15 mL) was added to a solution of **1** (1.0 g, 3.05 mmol) in THF (45 mL) and MeOH (30 mL). The resulting solution was heated at 60 °C for 1 h and cooled to room temperature. Methyl iodide (0. 57 mL) was added to the reaction mixture, and it was stirred at room temperature for 1h. The reaction mixture was poured into water and extracted with chloroform. The solvent was removed, and the residue was subjected to column chromatography (silica gel, ethyl acetate/hexane) to yield **2** (0.33 g, 68%). The spectral data of **2** were identical to those reported in the literature.[47]

H_2OMTP. Pyrrole **2** was converted into the porphyrin H_2OMTP in a 20% yield via formylation with $POCl_3$ and DMF, followed by a reduction with sodium borohydride and tetramerization with acid according to the literature procedure.[47] The spectral data of H_2-OMTP are identical to those of the literature.

NiOMTP. H_2OMTP was converted into the Ni complex by treating it with nickel acetate. A mixture of H_2OMTP (0.1 g) and $Ni(OAc)_2{\cdot}4H_2O$ (17 g) in MeOH (30 mL) and $CHCl_3$ (30 mL) was refluxed for 1 week. The reaction progress was monitored by UV−vis spectroscopy. The reaction mixture was poured into water and extracted with $CHCl_3$, followed by column chromatography (silica gel, $CHCl_3$) to give NiOMTP in a nearly quantitative yield as dark red microcrystals. ^{1}H NMR ($CDCl_3$): δ 3.04 (s, 24H, $-SCH_3$), 10.65 (s, 4H, $-C_mH-$). ^{13}C NMR ($CDCl_3$): δ 21.09 (s, SCH_3), 101.21 (s, C_β), 143.13 (s, C_α). MS (HRFAB-MS): *m*/*z* 734.3883 (M^+). Calcd for $C_{28}H_{28}N_4S_8Ni$: 733.9429. Anal. Calcd. for $C_{28}H_{28}N_4S_8Ni$: C, 45.71; H, 3.84; N, 7.61. Found: C, 45.82; H, 3.70; N, 7.73.

Quantum Chemical Calculations. All calculations have been performed with the ADF (Amsterdam Density Functional) suite of programs, release 2004.01.[48,49] The calculations made use of the local density approximation (LDA) functional of Vosko−Wilk−

(35) Antipas, A.; Gouterman, M. *J. Am. Chem. Soc.* **1983**, *105*, 4896.
(36) Gouterman, M. The Porphyrins. In *The Porphyrins*; Dolphin, D., Ed.; Academic Press: New York, 1978; Vol. 3, p 1.
(37) Rodriguez, J.; Holten, D. *J. Chem. Phys.* **1989**, *91*, 3525.
(38) Rodriguez, J.; Kirmaier, C.; Holten, D. *J. Am. Chem. Soc.* **1989**, *111*, 6500.
(39) Rodriguez, J.; Kirmaier, C.; Holten, D. *J. Chem. Phys.* **1991**, *94*, 6020.
(40) Kobayashi, T.; Straub, K. D.; Rentzepis, P. M. *Photochem. Photobiol.* **1979**, *29*, 925.
(41) Chirvony, V. S.; Dzhagarov, B. M.; Timinskii, Y. V.; Gurinovich, G. P. *Chem. Phys. Lett.* **1980**, *70*, 79.
(42) Chikisev, A. Y.; Kamalov, V. F.; Korteev, N. I.; Kvach, V. V.; Shkvrinov, A. P.; Toluetaev, B. N. *Chem. Phys. Lett.* **1988**, *144*, 90.
(43) Apanasevich, P. A.; Kvach, V. V.; Orlovich, V. A. *J. Raman Spectrosc.* **1989**, *20*, 125.
(44) Sato, S.; Kitiagawa, T. *Appl. Phys.* **1994**, *B59*, 415.
(45) Nikolaitchik, A. V.; Korth, O.; Rodgers, M. A. J. *J. Phys. Chem. A* **1999**, *103*, 7587.
(46) Pelliccioli, A. P.; Henbest, K.; Kwag, G.; Carvagno, T. R.; Kenney, M. E.; Rodgers, M. A. J. *J. Phys. Chem. A* **2001**, *105*, 1757.
(47) Jepperson, J. O.; Takimiya, K.; Jensen, F.; Brimert, T.; Nielsen, K.; Throup, N.; Becher, J. *J. Org. Chem.* **2000**, *65*, 5794.
(48) *ADF: Density Functional Theory (DFT) Software for Chemists.* Scientific Computing & Modelling: Amsterdam, http://www.scm.com, 2004.

Scheme 1 [a]

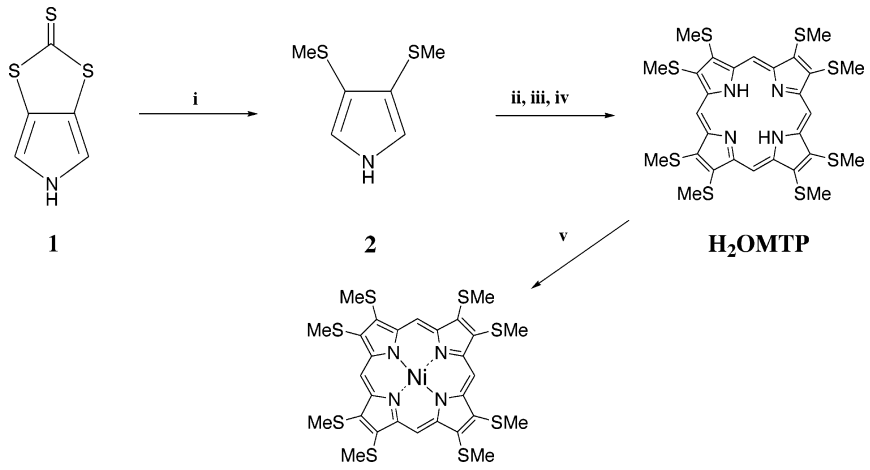

[a] Conditions: (i) NaH, MeOH−THF, MeI 68%; (ii) $POCl_3$, DMF; (iii) $NaBH_4$, Et_2O−MeOH; (iv) $CH_2(OMe)$, *p*-TsOH, DDQ, CH_2Cl_2; (v) $Ni(OAc)_2 \cdot 4H_2O$, MeOH−$CHCl_3$, 1 week.

Nusair (VWN)[50] and the generalized gradient approximation (GGA), employing Becke's[51] gradient approximation for exchange and Perdew's[52] for correlation (BP). The excitation energies were calculated using time-dependent density functional theory (TDDFT). In the ADF implementation,[53,54] the solution of the TDDFT response equations proceeds in an iterative fashion starting from the usual ground state or zero-order Kohn−Sham (KS) equations.[54] For these, one needs an approximation of the usual static exchange-correlation (xc) potential, $v_{xc}(\mathbf{r})$. After the ordinary KS equations have been solved, the first-order density change has to be calculated from an iterative solution to the first-order KS equations. In these first-order equations, an approximation is needed for the first functional derivative of the time-dependent xc potential, $v_{xc}(\mathbf{r}, t)$, with respect to the time-dependent density, $\rho(\mathbf{r}', t')$, the so-called xc kernel. For the xc kernel, we used the adiabatic local density approximation (ALDA). In this approximation, the time dependence (or frequency dependence referring to the Fourier-transformed kernel) is neglected, and one simply uses the differentiated static LDA expression. In our case, the Vosko−Wilk−Nusair parametrization was used.[50] For the exchange-correlation potentials, which appear in the zero-order KS equations, we employed the same GGA as in the DFT calculations. In all of the DFT and TDDFT calculations, the all-electron ADF TZ2P basis set, which is an uncontracted triple-ζ STO basis set with one 3d and one 4f polarization function for C, N, and S atoms, one 2p and one 3d polarization function for H, and a triple-ζ 3d, 4s basis with one 4p and one 4f function for Ni, was used.

The vertical absorption energies, E_{va}, have been evaluated at the ground-state optimized geometry. The adiabatic energies, E_{adia}, have been obtained according to the expression

$$E_{adia} = E_{ve} + \Delta E$$

where E_{ve} is the vertical emission energy, which is calculated at the TDDFT level using the relaxed excited-state geometry. The ΔE term accounts for the change in energy of the ground state upon deformation to the relaxed geometry of the excited state (for a schematic definition of the calculated energies, see Figure 10 in ref 55).

Geometry optimizations were performed for the ground state and selected triplet excited states of NiOMTP. Open-shell DFT calculations for the triplet states were performed within a spin-unrestricted formalism and spin contamination, monitored by the expectation value of S^2, was found to be negligible. The optimized ground- and excited-state triplet structures were verified to be true minima by frequency calculations. These calculations were performed at DFT/B88P86/6-31G(d) level of theory using the PQS 3.1 suite of programs.[56]

For the simulation of solvent effects on the ground-state geometries and excitation energies of NiOMTP, the conductor-like continuum solvent model (COSMO)[57−59] has been used.

The molecular orbitals were visualized with Molden 3.6,[60] and the ADF output data were converted to the Molden format using the ADF2MOLDEN program.[61]

Results and Discussion

Synthesis. Octakis-2,3,7,8,12,13,17,18-methylthioporphyrin, H_2OMTP, was prepared from **2** using the procedure of Sugiura and Sakata.[17] Their method for preparing **2** is based on the reaction of *N*-(triisopropylsilyl)-3,4-dibromopyrrole with *n*-BuLi followed by treatment with dimethyl disulfide. We have adopted another route for the preparation of **2** . This porphyrin building block was prepared by reaction of **1**[47] with methyl iodide in the presence of sodium methoxide. The conversion of H_2OMTP into the corresponding nickel(II) complex was carried out by refluxing a mixture

(49) te Velde, G.; Bickelhaupt, F. M.; Baerends, E. J.; van Gisbergen, S. J. A.; Guerra, C. F.; Snijders, J. G.; Ziegler, T. *J. Comput. Chem.* **2001**, *22*, 931.
(50) Vosko, S. H.; Wilk, L.; Nusair, M. *Canad. J. Phys.* **1980**, *58*, 1200.
(51) Becke, A. *Phys. Rev. A* **1988**, *38*, 3098.
(52) Perdew, J. P. *Phys. Rev. B* **1986**, *33*, 8822 (Erratum PRB 34 1986 7406).
(53) van Gisbergen, S. J. A.; Snijders, J. G.; Baerends, E. J. *Comput. Phys. Commun.* **1999**, *118*, 119.
(54) van Gisbergen, S. J. A.; Snijders, J. G.; Baerends, E. J. *J. Chem. Phys.* **1995**, *103*, 9347.
(55) Gunaratne, T. C.; Gusev, A. V.; Peng, X.; Rosa, A.; Ricciardi, G.; Baerends, E. J.; Rizzoli, C.; Kenney, M. E.; Rodgers, M. A. J. *J. Phys. Chem. A* **2005**, *109*, 2078.
(56) *PQS*, version 3.1; Parallel Quantum Solutions: Fayetteville, AR, 2004.
(57) Klamt, A.; Schürmann, G. *J. Chem. Soc., Perkin Trans.* **1993**, *2*, 799.
(58) Klamt, A.; Jonas, V. *J. Chem. Phys.* **1996**, *105*, 9972.
(59) Pye, C. C.; Ziegler, T. *Theor. Chem. Acc.* **1999**, *101*, 396.
(60) Schaftenaar, G.; Noordik, J. H. *J. Comput.-Aided Mol. Design* **2000**, *14*, 123.
(61) Volkov, A. V. *ADF2MOLDEN*. State University of New York: Buffalo, NY, 1999.

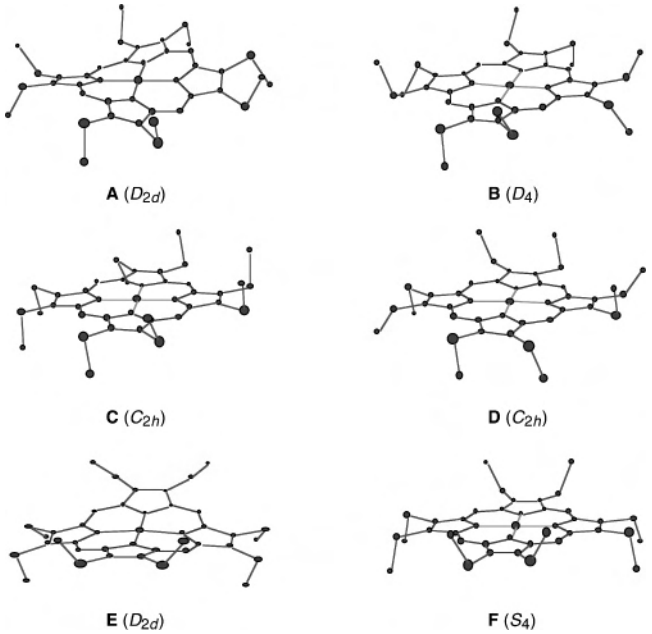

Figure 1. Structures of NiOMTP conformers showing the orientation of the methylthio groups and the type of distortion of the porphyrin core. Hydrogen atoms are omitted for clarity.

of H_2OMTP and $Ni(OAc)_2 \cdot 4H_2O$ in methanol and chloroform(Scheme 1).

Ground-State Molecular Structure. NiOMTP is expected to show rich conformational behavior because the tendency of Ni(II) porphyrins to deviate from planarity[34] coupled with the conformational flexibility of the eight methylthio groups can generate a number of conformers. In this study, we concentrate on the energy and geometry of the six NiOMTP conformers shown in Figure 1. We have been guided in the choice of these conformers by the structural behavior of related systems, viz., NiOEP,[25] NiP,[62] and ZnOMTP.[17] Initially, symmetry-constrained geometry optimizations were performed for the six conformers. The lowest energy was found for the ruffled conformer with D_{2d} symmetry, **A**. The planar conformer with D_4 symmetry, **B**, which is characterized by the same orientation of the vicinal methylthio groups (the methylthio substituents residing on the same pyrrolic subunit) as in **A**, is only 0.36 kcal/mol less stable, whereas conformers **C**, **D**, **E**, and **F** are 4.29, 4.78, 5.10, and 5.25 kcal/mol less stable than **A**, respectively.

The relative energies of the six optimized structures clearly indicate that the orientation of the vicinal methylthio groups has a significant impact on the stability of the NiOMTP conformers, the *ud* (*u*, up; *d*, down) orientation being preferred over the *uu* or *dd* orientations. Conformers **A** and **B**, which are characterized by a *ud* orientation of the methylthio groups, are indeed the most stable, whereas the saddled D_{2d} conformer, **E**, and the ruffled S_4 conformer, **F**, in which the vicinal methylthio groups are alternatively *uu* and *dd* are the highest in energy. The strong tendency of the vicinal methylthio substituents to assume a *ud* orientation is most likely dictated by the necessity of relieving the steric repulsion between the in-plane sulfur lone pairs.

Table 1. Relative Energies and Selected Bond Parameters of the Stable NiOMTP Conformers

parameter	D_{2d}-*ruf*	D_2	C_2	C_s	D_{2d}-*sad*	S_4
ΔE (kcal/mol)	0.00	0.31	2.31	4.77	5.10	5.20
Ni−N	1.9357	1.9411	1.9360	1.9408	1.9381	1.9365
C_α−N−N−C_α[a]	34.5	30.6	34.8	30.5	0.0	12.8
C_α−N−N−C_α[b]	0.0	1.2	1.2	0.0	13.8	13.1

[a] Torsional angle (deg) of the opposite pyrrole ring planes with respect to an axis through the nitrogen atom. [b] Torsional angle (deg) of the adjacent pyrrole ring planes.

For each NiOMTP conformer under consideration, frequency calculations were performed and analyzed. It was found that the optimized geometries of conformers **A**, **E**, and **F** correspond to stable energy minima (all positive harmonic frequencies), whereas the optimized geometries of conformers **B**, **C**, and **D** have one imaginary frequency associated with ruffling of the porphyrin core. The geometries of conformers **B**, **C**, and **D** were therefore distorted along the eigenvector representing the imaginary frequency and reoptimized, and the frequencies were recalculated. The theoretical results show that the minimum corresponding to conformer **B** has a ruffled structure of D_2 symmetry and the minimum corresponding to conformer **C** has a ruffled structure of C_s symmetry, whereas the distortion of conformer **D** leads to a ruffled structure of C_2 symmetry. The ruffling lowers the energy of conformers **B** and **D** by only 0.01 and 0.10 kcal/mol, respectively. A trivial gain in energy upon ruffling was also predicted for NiP[62] and NiOEP[25] by DFT/B3LYP calculations. In contrast with conformers **B** and **D**, conformer **C** is significantly (2.00 kcal/mol) stabilized upon ruffling of the porphyrin core. The "anomalously" large stabilization of conformer **C** upon ruffling can be understood in terms of the relief of the steric repulsion between the vicinal sulfur lone pairs being particularly large because of the *uu*−*dd*−*dd*−*uu* orientation of the methylthio groups.

The relative energies and the most relevant structural parameters of the six stable NiOMTP conformers are reported in Table 1.

As can be inferred from this table, the nearly degenerate D_{2d} and D_2 ruffled conformations (the D_2 conformation is only 0.36 kcal/mol less stable than the D_{2d} conformation), both characterized by a *ud* orientation of the methylthio groups, are by far the preferred ones in the "gas phase". The other conformers, which are characterized by *uu* and *dd* orientations of the methylthio groups, are 2.0−5.0 kcal/mol higher in energy. These results unambiguously indicate that it is the orientation of the vicinal methylthio groups rather than the type and degree of distortions of the porphyrin core that determines the stability of the NiOMTP conformers in the gas phase. It is not so for NiOEP, the most stable conformers of which were theoretically predicted to be substantially degenerate, regardless of the orientation assumed by the vicinal ethyl groups.[25]

Because the optical and photophysical measurements on NiOMTP were performed in a condensed phase (toluene solution), we have also considered the effects of the solvent

(62) Kozlowski, P. M.; Rush, T. S., III; Jarzecki, A. A.; Zgierski, M. Z.; Chase, B.; Piffat, C.; Ye, B.-H.; Li, X.-Y.; Pulay, P.; Spiro, T. G. *J. Phys. Chem. A* **1999**, *103*, 1357.

Table 2. Selected Bond Lengths (Å) and Bond Angles (deg) Calculated for NiOMTP in the Ruffled D_{2d} Conformation Are Compared with Those Calculated and Experimentally Determined for NiP

	NiOMTP	NiP		
	BP/TZ2P[a]	BP/TZ2P[a,b,c]	B3LYP/ 6-311G(d)[b,d]	X-ray[e]
Ni−N	1.9357	1.9462 (1.9651)	1.9577	1.951(2)
N−C_α	1.3769	1.3803 (1.3816)	1.3758	1.379(2)
C_α−C_β	1.4512	1.4395 (1.4386)	1.4386	1.435(4)
C_β−C_β	1.3814	1.3616 (1.3600)	1.3563	1.347(3)
C_α−C_m	1.3820	1.3816 (1.3789)	1.3809	1.371(3)
C_β−S	1.7573			
S−C_{Me}	1.8312			
C_α−C_m−C_α	122.73	123.06 (123.58)	123.46	123.5(2)
C_α−N−C_α	105.93	105.03 (104.51)	104.98	104.3(2)
N−C_α−C_β	110.68	110.73 (111.09)	110.81	111.0(3)
C_α−C_β−C_β	106.32	106.72 (106.66)	106.69	106.8(2)
C_β−C_β−S	130.08			
C_β−C_β−S−C_{Me}	60.03			
C_α−N−N−C_α[f]	34.47	25.38 (0.0)	19.62	1.7

[a] This work. [b] D_{2d} symmetry. [c] Numbers in parentheses refer to the planar (D_{4h}) conformation. [d] From ref 62. [e] From ref 24. [f] Torsional angle (deg) of the opposite pyrrole ring planes with respect to an axis through the nitrogen atoms.

on the geometry and relative stabilities of the two most stable conformers. Starting from the gas-phase geometries, we reoptimized the structures of the ruffled D_{2d} and D_2 NiOMTP conformers with a COSMO correction. The solvation has a negligible effect on the geometry of the two conformers, as for their relative energies, and the D_2 conformer is still slightly less stable (0.45 kcal/mol) than the D_{2d} conformer. Although the very small energy gap ($\sim RT$ at room temperature) between the NiOMTP ruffled conformers of D_{2d} and D_2 symmetry makes them both accessible in solution, we restricted the ground- and excited-state theoretical studies to the most stable conformer, D_{2d}. The nearly degenerate D_2 conformer indeed has a very similar molecular structure and is not expected to have significantly different ground- and excited-state properties.

The structural parameters calculated for the ruffled NiOMTP conformer of D_{2d} symmetry are gathered in Table 2 and compared with those calculated and experimentally[24] determined for the parent NiP. Previous[62] and present DFT calculations on NiP show that the lowest-energy structure is a true minimum with D_{2d} symmetry. It is slightly distorted from the planar geometry along the ruffling coordinate. The planar D_{4h} structure is unstable with respect to ruffling distortion, although it is only ~0.1 kcal/mol less stable. As can be inferred from the data in Table 2, the DFT-computed geometries are in good agreement with crystallographically determined values, except for the degree of ruffling, which is predicted to be significantly larger than the experimental value of 2°. As previously suggested,[62] the discrepancy between theory and experiment can be attributed to crystal packing forces, which can easily overcome the very soft ruffling potential predicted for NiP. The marked sensitivity of the calculated degree of ruffling to the level of theory (cf. Table 2) can be also traced to the very soft ruffling potential.

The ruffling distortion of the porphyrin core increases by ~9° going from NiP to NiOMTP, as an effect of the steric conflicts of the peripheral methylthio groups, which are also responsible for the perceptible lengthening of the C_β−C_β bonds. As expected, the enhancement of the ruffling distortion correlates with the shortening of the Ni−N distance that is predicted in NiOMTP (~0.01 Å shorter than in NiP).

Ground-State Electronic Structure. The highest-occupied and lowest-unoccupied ground-state one-electron levels calculated for NiOMTP are shown in Figure 2, and an atomic orbital population analysis is given in Table 3. The ground-state electronic structure of NiOMTP can be understood in terms of the methylthio substituents inducing structural and electronic perturbations on NiP. The impact of ruffling the porphyrin core was evaluated by analyzing the electronic structure of NiP in the following conformations: (i) the optimized planar (D_{4h}) conformation, *planar*; (ii) the optimized ruffled (D_{2d}) conformation, *ruf*; and (iii) a ruffled conformation optimized by constraining the ruffling dihedral angles to the value they assume in NiOMTP, *ruf*-1. The impact of the bond angle and bond length changes induced by peripheral substituents, the so-called in-plane nuclear reorganization (IPNR),[63] was evaluated by analyzing the electronic structure of NiP in a ruffled conformation derived from the optimized NiOMTP structure, replacing the methylthio groups by hydrogen atoms (C−H bond length = 1.09 Å), *ruf*-2. Finally, the electronic methylthio group effects will become apparent from a comparison of NiP in the *ruf*-2 conformation with the computed orbital levels of NiOMTP. The one-electron levels of the four NiP conformers are shown in Figure 2, and their energies are gathered in Table 4.

Considering first the *planar* form of NiP, among the one-electron levels in Figure 2, one may recognize the occupied $5a_{2u}$ and $1a_{1u}$, the unoccupied $5e_g$ (the G orbitals, where G = Gouterman), and the metal 3d orbitals. In the virtual spectrum, there is the $3d_{x^2-y^2}$ ($10b_{1g}$) orbital, which is pushed up by antibonding with the N lone pairs. According to the orbital composition (see Table S1), the $3d_{x^2-y^2}$ orbital is strongly mixed with the N lone pairs.

The highest-occupied 3d levels are the nearly degenerate $4e_g$ ($3d_\pi$) and $15a_{1g}$ ($3d_{z^2}$). The latter is an almost pure metal orbital, largely (89%) $3d_{z^2}$, with some (9%) 4s character and a small antibonding admixture of the N $2p_x$. The former is heavily mixed with the N-based π orbitals of the porphyrin ring, its bonding counterpart, the $3e_g$, lying 1.7 eV below. The Ni $3d_{xy}$, which in our coordinate system points to the bridging methines, occurs mostly (93%) in the $9b_{2g}$.

(63) Wertsching, A. K.; Koch, A. S.; DiMagno, S. G. *J. Am. Chem. Soc.* **2001**, *123*, 3932.

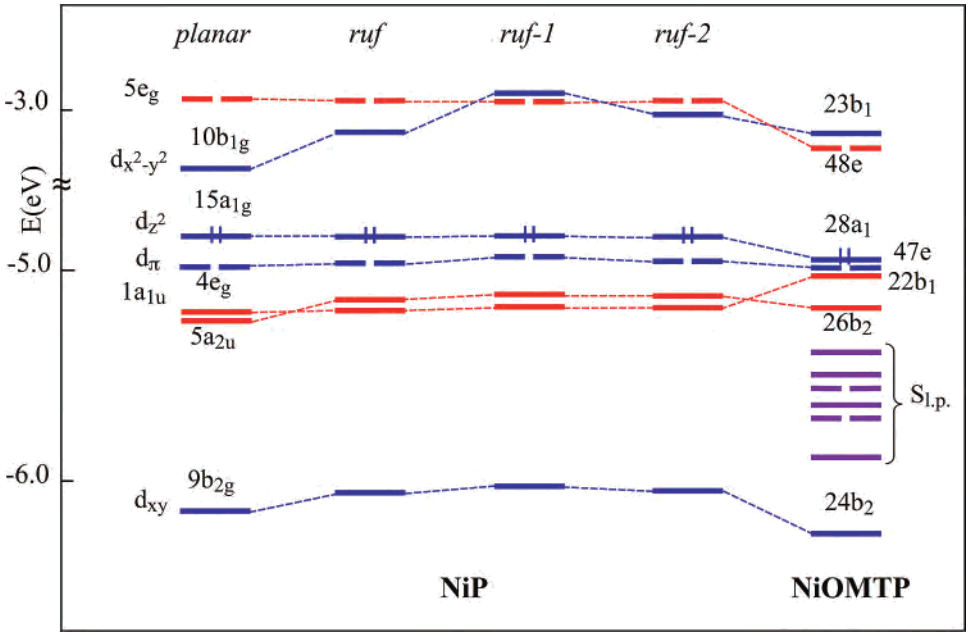

Figure 2. Energy level scheme for NiP and NiOMTP.

Table 3. Energies and Percentage Composition of the Highest-Occupied and Lowest-Unoccupied Molecular Orbitals of NiOMTP Expressed in Terms of Individual Atoms[a]

MO	*E* (eV)	Ni	N	C_α	C_β	C_m	S
			unoccupied				
$23b_1$	−3.14	55 ($d_{x^2-y^2}$)	32 (lp)	3	5		2
48e	−3.19	3 (d_π)	12 ($2p_z$)	18 ($2p_z$)	24 ($2p_z$)	26 ($2p_z$)	5
			occupied				
$28a_1$	−5.00	87 (d_{z^2})	2				
		10 (4s)					
47e	−5.02	53 (d_π)	7 ($2p_z$)	4 ($2p_z$)	14 ($2p_z$)		13 (lp)
$22b_1$	−5.07	2 ($d_{x^2-y^2}$)		45 ($2p_z$)	11 ($2p_z$)		33 (lp)
$26b_2$	−5.20		17 ($2p_z$)	5 ($2p_z$)	10 ($2p_z$)	50 ($2p_z$)	9 (lp)
$20a_2$	−5.43		11 ($2p_{z,x}$)		19 ($2p_z$)		59 (lp)
$25b_2$	−5.52	8 (d_{xy})	14($2p_z$)		10 ($2p_z$)	3 ($2p_z$)	55 (lp)
46e	−5.57			3 ($2p_z$)	4 ($2p_z$)	2 ($2p_z$)	75 (lp)
$27a_1$	−5.67	2 (d_{z^2})					
45e	−5.73	26 (d_π)	2 ($2p_z$)	2 ($2p_z$)	4 ($2p_z$)		56 (lp)
$21b_1$	−5.92			21 ($2p_z$)	19 ($2p_z$)		46 (lp)
$24b_2$	−6.27	75 (d_{xy})		4 ($2p_{z,y}$)		4 ($2p_{z,x}$)	9 (lp)

[a] The hydrogen and methyl carbon contribution to these orbitals is almost negligible.

Table 4. Energies of the Highest-Occupied and Lowest-Unoccupied MOs for NiP in Different Conformations

MOs D_{4h}/D_{2d}	*planar*	*ruf*	*ruf*-1	*ruf*-2
$5e_g/24e$	−2.95	−2.96	−2.96	−2.97
$10b_{1g}/11b_1$	−3.28	−3.10	−2.95	−3.02
$15a_{1g}/16a_1$	−4.88	−4.86	−4.84	−4.86
$4e_g/23e$	−5.01	−4.98	−4.95	−4.98
$5a_{2u}/14b_2$	−5.20	−5.16	−5.12	−5.13
$1a_{1u}/10b_1$	−5.19	−5.18	−5.17	−5.17
$9b_{2g}/13b_2$	−6.15	−6.07	−6.02	−6.05

It is worthwhile to note that we find, with the present BP functional, the two highest-occupied metal d states lying *higher* than the occupied Gouterman orbitals. This ordering is reversed compared to that of the more elaborate, asymptotically correct, SAOP potential[64,65] we used earlier.[30,66−68] Compared to the pure LDA and GGA potentials, the SAOP potential has been found to perform particularly well for excitation with Rydberg and mixed Rydberg−valence character, which is apparently the result of the improved shape in the outer regions of the molecules. For pure valence transitions, it has a much smaller effect. In the present study, we are dealing with pure valence excitations and, moreover, the relative position of the d levels with respect to the ring levels is crucially important. As stressed in our previous papers,[30,67,68] the metal based MOs experience a significant unwarranted downshift upon changing from the BP to the SAOP potential. For this reason, the BP potential has been retained in this work. Hybrid potentials, such as B3LYP, exhibit even more significant deviant behavior where d levels are concerned, so we will address the important issue of the problems of various DFT functionals with respect to the position of the d levels and the related MLCT and d−d excitation energies, in a separate paper.[69]

For the *ruf* form of NiP, according to the level scheme of Figure 2 and the one-electron energies in Table 4, a 24° ruffling distortion of the porphyrin core destabilizes the G a_{2u} and all of the metal states, particularly the $10b_{1g}$ ($d_{x^2-y^2}$) and the $9b_{2g}$ (d_{xy}).

The ruffling-induced contraction of the porphyrin cavity (the Ni−N bond length decreases by ∼0.02 Å going from the *planar* to the *ruf* conformer, cf. Table 2) accounts well for the destabilization of the $10b_{1g}$, $15a_{1g}$, and $4e_g$ orbitals, all of which have nickel−macrocycle antibonding character, while the upshift of the $9b_{2g}$ has to be traced to accidental

(64) Gritsenko, O. V.; Schipper, P. R. T.; Baerends, E. J. *Chem. Phys. Lett.* **1999**, *302*, 199.
(65) Schipper, P. R. T.; Gritsenko, O. V.; van Gisbergen, S. J. A.; Baerends, E. J. *J. Chem. Phys.* **2000**, *112*, 1344.
(66) Rosa, A.; Baerends, E. J. *Inorg. Chem.* **1994**, *33*, 584.
(67) Baerends, E. J.; Ricciardi, G.; Rosa, A.; van Gisbergen, S. J. A. *Coord. Chem. Rev.* **2002**, *230*, 5.
(68) Rosa, A.; Ricciardi, G.; Gritsenko, O.; Baerends, E. J. *Struct. Bond.* **2004**, *112*, 49.
(69) Baerends, E. J.; Rosa, A.; Ricciardi, G. Manuscript in preparation.

mixing upon ruffling of the Ni d_{xy} orbital with the C_β and C_m $2p_z$ orbitals.

Providing an explanation for the upshift of the G a_{2u} is much less straightforward. This issue has recently been addressed by Evans and Musselman[23] for the specific case of NiOEP. On the basis of semiempirical (ZINDO) calculations, these authors trace the ruffling-induced upshift of the G a_{2u} primarily to the reduced overlap between the C_α and C_m $2p_z$ orbitals, although they consider the decreased overlap between the Ni $4p_z$ and the N $2p_z$ orbitals, caused by the tilting of the pyrrole ring, a likely contributing factor. Our DFT calculations fully support this interpretation.

As inferred from the one-electron energies of the *ruf*-1 conformer, an increase of the degree of ruffling up to ca. 34°, the value calculated for NiOMTP, further destabilizes the G a_{2u} and metal states. Of these, the Ni $3d_{x^2-y^2}$ ($11b_1$) is particularly destabilized (it ends up slightly above the G 24e) because of the Ni−N distance in the *ruf*-1 structure is significantly shorter than that in the *ruf* structure (1.9313 vs 1.9462 Å).

An estimate of the IPNR impact on the electronic structure of NiP can be achieved by comparing the one-electron energies of the *ruf*-2 and *ruf*-1 conformers. The data in Table 4 clearly show that IPNR has a negligible impact. The Gouterman levels remain almost unaltered and the metal states only experience a modest stabilization as a result of the slight lengthening of the Ni−N bond distance (1.9357 vs 1.9313 Å).

When the orbital levels of NiP in the *ruf*-2 conformation are compared with those of NiOMTP (Figure 2), the genuine electronic effects of the methylthio groups become apparent. Replacing hydrogen atoms with methylthio groups induces a general, although not uniform, downward shift of all levels except for the Gouterman $22b_1$, which is strongly destabilized. The considerable upshift of the $22b_1$ state can be traced to antibonding (visible in the plot of this orbital in Figure 3) between the C_β $2p_z$ and the sulfur lone pairs, whose contribution to this orbital amounts to ∼33% (Table 3). The other occupied G level, the $26b_2$, also has some C_β $2p_z/S_{l.p.}$ antibonding character (cf. the plot of this orbital in Figure 3). Nevertheless, unlike the $22b_1$, it is slightly stabilized because the above-mentioned stabilizing effect of the methylthio groups is the prevailing one. Thus, in NiOMTP, the occupied Gouterman orbitals are in an inverted order with respect to NiP (*ruf*-2) and are no longer degenerate. As for the unoccupied G 48e level, it is stabilized to a sizable extent and ends up below the Ni $3d_{x^2-y^2}$, becoming the LUMO in NiOMTP.

The introduction of the methylthio groups does not modify the salient features of the nickel−porphyrin interactions. However, the energy and composition of the metal states, to some extent, sense the change in the relative energy of the macrocycle and the metal orbitals leading to a differential stabilization of the occupied metal orbitals. According to the atomic orbital population analysis in Table 3 and the orbital scheme of Figure 2, the methylthio groups introduce additional levels with sulfur lone-pair character in the valence region.

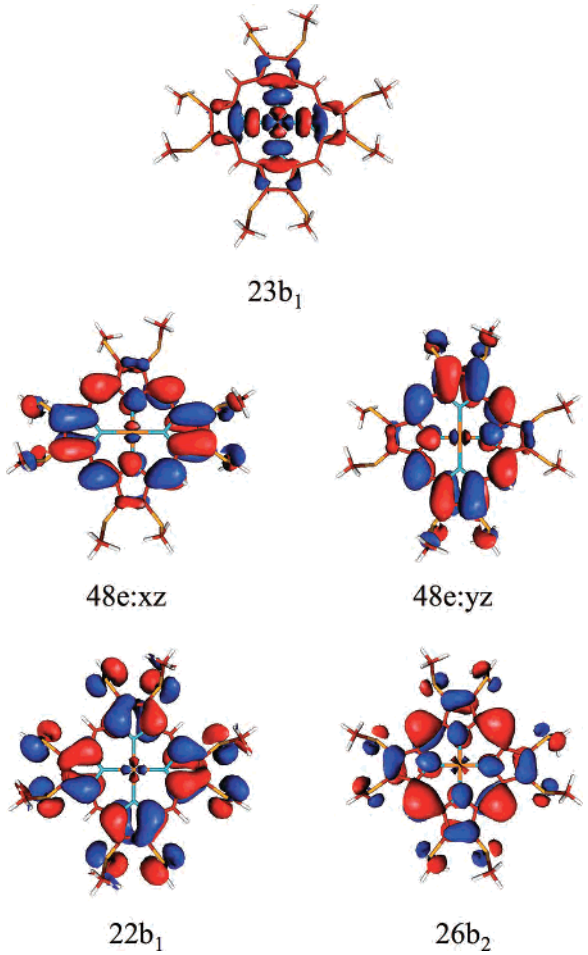

Figure 3. Contour plots of the $23b_1$, 48e (LUMOs), $22b_1$ and $26b_2$ orbitals of NiOMTP.

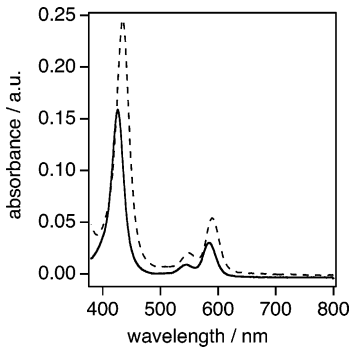

Figure 4. Optical absorption spectra of NiOMTP in toluene (full line) and CS_2 (dashed line).

Excited States and Optical Spectra. Figure 4 shows the ground-state absorption spectra of NiOMTP recorded in toluene and in CS_2 at room temperature. The spectra are characterized by two clear vibrational progression peaks of sizable intensity in the visible region corresponding to the Q(0,0) and Q(1,0) bands, an intense absorption in the near UV, the Soret (B) band, and a weak continuum absorption in between. The spectral features, especially the Soret band, show appreciable solvatochromism. Relative to the parent NiP and the ethyl-substituted analogue, NiOEP, NiOMTP exhibits red-shifted Q and B bands. A comparison of the UV−vis absorption spectra of NiOMTP and NiP in CS_2

Table 5. TDDFT Vertical Excitation Energies (eV/nm) of the Lowest Optically Allowed Excited States of NiP in the Planar and Ruffled Conformations with an Oscillator Strength (*f*) Larger than 0.001 Compared to the Experimental Data[a]

D_{4h}				D_{2d}				
state	composition (%)	E_{va}	*f*	state	composition (%)	E_{va}	*f*	exptl[b]
1^1E_u	51 ($1a_{1u} \rightarrow 5e_g$)	2.41/514	0.0055	3^1E	48 ($10b_1 \rightarrow 24e$)	2.38/521	0.0038	2.28/543
	48 ($5a_{2u} \rightarrow 5e_g$)				48 ($14b_2 \rightarrow 24e$)			Q
2^1E_u	34 ($5a_{2u} \rightarrow 5e_g$)	3.18/390	0.6404	4^1E	41 ($13b_2 \rightarrow 24e$)	3.06/405	0.3608	3.11/399
	32 ($1a_{1u} \rightarrow 5e_g$)				25 ($10b_1 \rightarrow 24e$)			B
	29 ($4e_g \rightarrow 2b_{1u}$)				23 ($14b_2 \rightarrow 24e$)			

[a] The major one-electron transitions contributing to the BP/LDA solution vectors are also given. [b] Data taken in CS_2 solution, from ref 24.

Table 6. TDDFT Vertical Excitation Energies (eV/nm) of the Lowest Optically Allowed Excited States of NiOMTP with an Oscillator Strength (*f*) Larger than 0.001 Compared to the Experimental Data[a]

state	composition (%)	E_{va}	f	exptl
2^1E	68 ($22b_1 \rightarrow 48e$), 26 ($26b_2 \rightarrow 48e$)	2.04/608	0.0964	2.10/590,[b] 2.12/585[c] Q
4^1E	69 (**$20a_2$**$\rightarrow 48e$), 13 (**$25b_2$**$\rightarrow 23b_1$)	2.30/539	0.0764	
5^1E	34 (**$25b_2$**$\rightarrow 48e$), 25 (**$20a_2$**$\rightarrow 48e$), 16 (**46e**$\rightarrow 23b_1$), 16 ($26b_2 \rightarrow 48e$)	2.38/521	0.0608	
7^1E	88 (**$27a_1$**$\rightarrow 48e$)	2.51/494	0.0157	
8^1E	24 (**46e**$\rightarrow 23b_1$), 23 (**$21b_1$**$\rightarrow 48e$), 21 ($26b_2 \rightarrow 48e$), 8 (**$25b_2$**$\rightarrow 48e$), 7 ($22b_1 \rightarrow 48e$)	2.58/481	0.3499	
9^1E	66 ($47e \rightarrow 29a_1$), 16 (**45e**$\rightarrow 23b_1$), 11 (**$21b_1$**$\rightarrow 48e$)	2.81/441	0.0084	
11^1E	32 (**$21b_1$**$\rightarrow 48e$), 31 ($24b_2 \rightarrow 48e$), 11 ($47e \rightarrow 29a_1$), 8 ($26b_2 \rightarrow 48e$), 7 ($22b_1 \rightarrow 48e$)	3.02/411	0.7312	2.85/435,[b] 2.92/424[c] B
12^1E	57 ($24b_2 \rightarrow 48e$), 12 (**46e**$\rightarrow 29a_1$), 10 (**$21b_1$**$\rightarrow 48e$), 7 ($26b_2 \rightarrow 48e$), 4 ($22b_1 \rightarrow 48e$)	3.23/384	0.7064	

[a] The major one-electron transitions contributing to the BP/LDA solution vectors are also given, and the sulfur lone pair-based MOs are printed in bold face. [b] Data taken in CS_2 solution, this work. [c] Data taken in toluene solution, this work.

Table 7. Vertical Excitation Energies (eV) Calculated for the Q and B Bands of the NiP Conformers

	planar	*ruf*	*ruf*-1	*ruf*-2
Q	2.41	2.38	2.35	2.35
B	3.18	3.06	3.00	3.00

reveals that methylthio substitution induces a bathochromic shift of the Q(0,0) and B bands of 47 and 36 nm, respectively.

To understand the origin of the considerable red shift of the UV−vis features in the optical spectra of NiOMTP, we performed TDDFT calculations for the lowest optically allowed excited states of NiOMTP and NiP in the *planar*, *ruf*, *ruf*-1, and *ruf*-2 conformations. Solution calculations, including the COSMO solvation correction, were carried out for the excited states of NiOMTP using the structure optimized in toluene to model the photophysical experiments in toluene. As could be expected for a solvent with a very low dielectric constant ($\epsilon = 2.38$), the solvation correction only causes a very small red shift (≤ 0.04 eV) of the calculated excitation energies. Therefore, only the gas-phase results are discussed in the following.

Tables 5 and 6 list the vertical absorption energies (E_{va}) and oscillator strengths (*f*) computed for NiP in the *planar* and *ruf* conformations and for NiOMTP in its most stable D_{2d} ruffled conformation. These tables also include the composition of the BP/ALDA solution vectors in terms of the major one-electron MO transitions. Table 7 provides a comparison of the excitation energies of the Q and B bands computed for NiP in the four conformations.

Considering first NiP as the point of reference for NiOMOTP, the TDDFT results in Table 5 show that the ruffling distortion has a significant impact on the energy of the excited states responsible for the Q(0,0) and B bands, the excitation energies computed for the *ruf* conformer being more in line with the experiment. Upon going from the *planar* to the *ruf* form, the Q and B states shift to the red by 7 and 14 nm, respectively. The ruffling-induced upshift of the a_{2u} and the consequent reduced a_{2u}/e_g energy gap causes the low-energy combination of the $a_{1u}(b_1) \rightarrow e_g(e)$ and $a_{2u}(b_2) \rightarrow e_g(e)$ G transitions, which accounts for the Q state occuring at lower energy in the *ruf* conformer. The same argument holds for the B state that, although having a mixed $\pi\pi^*$/MLCT character, is mainly accounted for by the high-energy combination of the Gouterman transitions. It should be noted, however, that for symmetry reasons the MLCT transition contributing to the B state both has a different weight and involves different MOs in the two conformers (cf. the composition of the 4^1E and 2^1E_u states in Table 5). The change in the composition of the B state on going from the *planar* to the *ruf* conformer is a likely contributing factor to the calculated red shift and is at the origin of the decreased intensity of this state in the *ruf* conformer.

According to the TDDFT results in Table 7, a further increase of the ruffling deformation, as it occurs on going from the *ruf* to the *ruf*-1 structure of NiP, shifts the Q and B bands by only 0.03 and 0.06 eV, respectively. A comparison of the excitation energies calculated for NiP in the *ruf*-1 and *ruf*-2 conformations shows that IPNR has no impact on the Q and B features. Therefore, the red shifts of the Q and B bands of NiOMTP relative to NiP appear to originate largely from genuine electronic effects from the peripheral methylthio groups. This could have already been suspected from the ground-state electronic structure analysis of NiOMTP and NiP in the planar and ruffled conformations, but it is amply confirmed by the explicit calculation of the excited states.

According to the TDDFT results presented in Table 6, the partial lifting of the G $a_{1u}(22b_1)$ and G $a_{2u}(26b_2)$ degeneracy induced by the upshift of the former causes the mixing of the Gouterman one-electron transitions to be much less effective in NiOMTP than in NiP, where it is close to 50−50. In NiOMTP, the 2^1E excited state responsible for the Q

band is mostly described by the $22b_1 \rightarrow 48e$, the transition out of the G a_{2u} MO, the $26b_2 \rightarrow 48e$, entering this state with only a 26% weight. As a consequence, the cancellation of the transition dipoles of the Gouterman transitions that occur in the Q state in NiP, leading to very low intensity of the Q band, occurs to a lesser extent in NiOMTP where this band has, in agreement with the experiment, appreciable intensity ($f = 0.0964$). The upshift of the G a_{1u} derived $22b_1$ and the downshift of the G e_g derived 48e also cause the low-energy combination of the Gouterman transitions that accounts for the Q band to be in NiOMTP at lower energy than in NiP.

In the region between the Q(0,0) and B bands, we predict several excited states with SPCT (sulfur-to-porphyrin charge transfer) character,[70] the most intense of which, the 4, 5, and 7^1E (cf. Table 6), are responsible for the increase in the nonzero absorption between the Q(1,0) and the B band. In the energy regime of the broad B band (470−380 nm), five excited states were computed. Three of these, the 8^1E, 11^1E, and 12^1E, at 2.58 eV (481 nm), 3.02 eV (411 nm), and 3.23 (384 nm), respectively, have large oscillator strengths and are therefore responsible for the intensity of this band. According to their composition, these states result from a configuration interaction between the high-energy combination of the G transitions, which is actually dominated by the $26b_2 \rightarrow 48e$, and nearly degenerate SPCT and MLCT transitions. Although, in the excited states responsible for the Soret band, the $22b_1 \rightarrow 48e$ G transition enters with only a minor weight, its contribution to the B states is sufficient to drive the high-energy combination of the Gouterman transitions to a lower energy than that in NiP. This contributes to the observed bathochromic shift of the B band in NiOMTP relative to NiP.

Photophysics. (a) Spectral Observations. Photoexcitation studies were carried out using excitation wavelengths of 400 nm, on the blue side of the Soret band, and 582 nm, in the Q-band envelope. Pulsed-light excitation generated transient spectral features throughout the 375 nm to 800 nm spectral region (see below). However, scattered light from the excitation beam caused significant interference in the data presentation. To obviate this for clean observations in the Q-band absorption region (500 nm to 750 nm), excitation at 400 nm was employed. To obtain a clearer picture of the 380 nm to 550 nm spectral region, excitation at 582 nm was employed. These different experiments are presented separately.

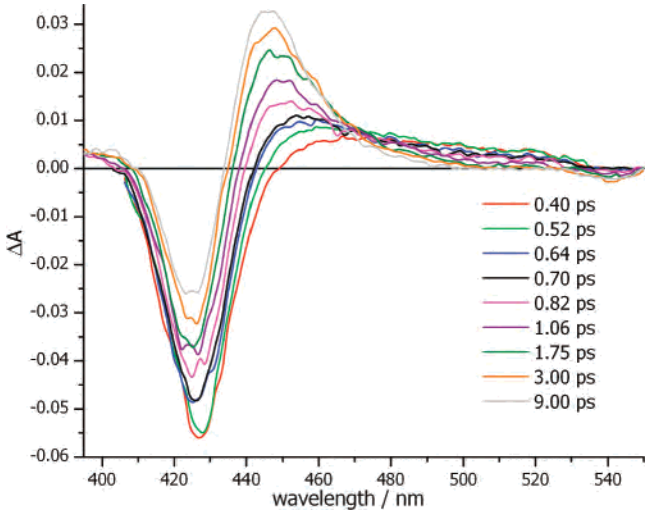

Figure 5. Nine spectral cuts (ΔA vs λ) at the indicated times from the transient dynamic surface generated upon excitation at 582 nm of NiOMTP (10 μM) in toluene.

Excitation at 582 nm. A solution of NiOMTP (ca. 5 μM) in toluene was excited with ca. 100 fs pulses of 582 nm light, and the optical dynamic surface, $\Delta A(\lambda, t)$ was recorded over a time window of 10 ps. As shown in Figure 4, this wavelength is close to the peak of the Q(0,0) band in the ground-state optical absorption spectrum of NiOMTP. Figure 5 shows nine spectral cuts taken from the dynamic surface, recorded over the range of 0.4 ps to 9 ps after the pulse and over the spectral range of 380 nm to 550 nm. The data have been subjected to a correction for chirp. The first observed transient (FOT) recorded at 400 fs shows a strong negative absorption signal in the Soret band region of the ground-state spectrum and a positive absorption with a broad maximum near 470 nm. The subsequent spectra (up to 9 ps) also show bleaching at the Soret region and a positive absorption at the red edge, with the maximum exhibiting a distinct blue shift as time proceeded.

Excitation at 400 nm. Solutions of NiOMTP (ca. 5 μM) in toluene were irradiated with ca. 100 fs pulses of 400 nm light, and the optical dynamic surface, $\Delta A(\lambda, t)$ was recorded over a time window up to 1.6 ns.

The first 10 ps of such a surface are displayed in Figure 6 (corrected for chirp), and Figure 7 shows a series of spectral cuts taken from the data of Figure 6 at a series of delay times. Scrutiny of the dynamic surface in Figure 6 shows a richness of spectral features connected by several dynamic processes within the depicted 10 ps window.

Regions of positive and negative difference absorption intersperse across the spectral region. Negative difference absorptions are seen in the 525−560 nm region and in the 575−610 nm region. These correspond to the ground-state

(70) The calculated excitation energies of these states are not expected to suffer the well-known failure of TDDFT in predicting the excitation energies of long-range charge-transfer states correctly (see refs 71−73). This is true for the excited states classified in this paper as LMCT or MLCT. The classification in terms of SPCT, LMCT, and MLCT is performed only on the basis of the character of the orbitals involved in the transitions. In the excitations with which we are dealing, no net charge transfer occurs from one moiety to another moiety of the complex, but a reorganization of the electronic density within the macrocycle or the metal orbitals does occur. As stressed in ref 68, this happens quite frequently in the so-called charge-transfer states (LL′CT, LMCT, MLCT) of transition metal complexes. For instance, the excitation of an electron out of a ligand orbital to a (mostly) d orbital is often accompanied by a change in the composition of the other orbitals (the "passive" orbitals) in such a way that the total d population remains practically the same. This is a consequence of the strong d−d repulsion. Exciting an electron from a ligand orbital to the d shell in a one-electron transition will increase the d population. However, this increased d population will destabilize the d levels with the effect that the d mixing into other occupied ligand orbitals diminishes, which has the effect of decreasing the total d population. The net effect is usually very little change in the d population.

(71) Dreuw, A.; Weisman, J. L.; Head-Gordon, M. *J. Chem. Phys.* **2003**, *119*, 2943.
(72) Dreuw, A.; Head-Gordon, M. *J. Am. Chem. Soc.* **2004**, *126*, 4007.
(73) Gritsenko, O.; Baerends, E. J. *J. Chem. Phys.* **2004**, *112*, 655.

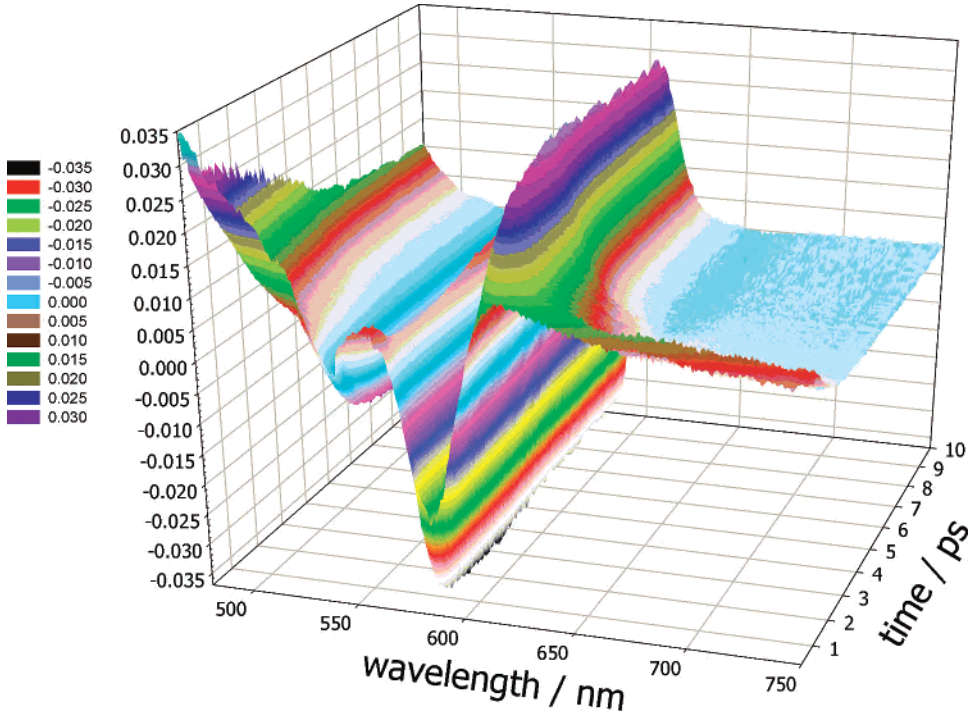

Figure 6. Perspective view of the first 10 ps of the $A(\lambda,t)$ surface collected during a pump−probe experiment of 10 μM NiOMTP in toluene. The excitation wavelength was 400 nm and the data have been corrected for chirp.

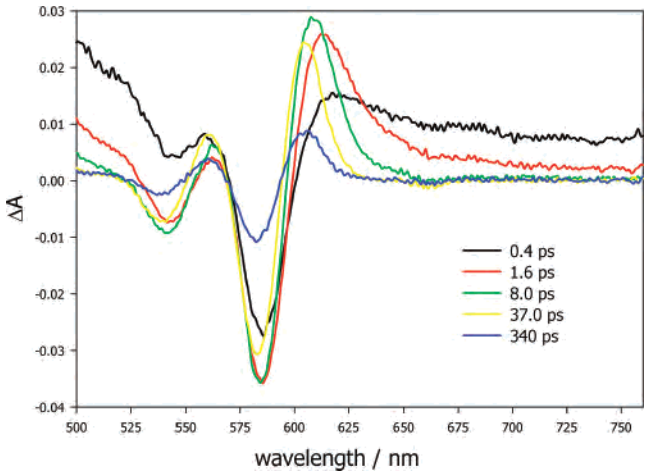

Figure 7. Five spectral cuts (ΔA vs λ) at the indicated times from the surface presented in Figure 6.

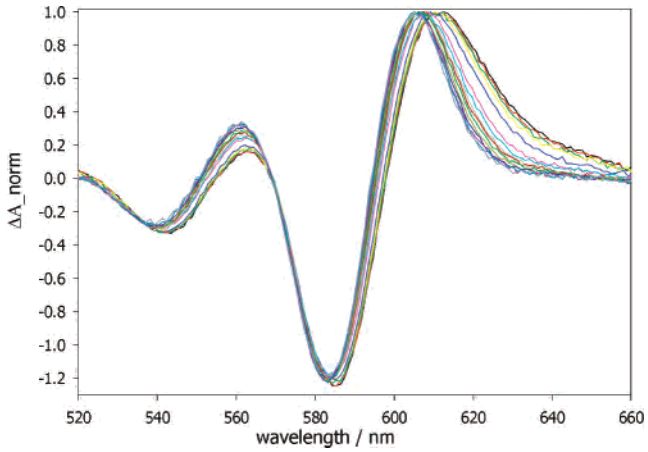

Figure 8. Series of spectral cuts from the surface in Figure 6 in the time range of 1−40 ps, normalized at the red-most maximum to clearly show the time-dependent blue shift.

absorption peaks in the same regions (Figure 4) and result from the conversion of ground state molecules into an excited state where the extinction coefficient of the ground state removed exceeds that of the product state formed in the regions of negative difference absorbance. In corollary, in the regions with a positive difference absorption, the extinction coefficient of the product state exceeds that of the removed ground state. Moreover, the positive absorption bands are very broad at early times but rapidly become narrower with the maxima shifting to the blue slightly. This blue shift is observed very clearly in Figure 8 in which the spectra between 4 and ca. 40 ps have been normalized at their red-most maximum.

Figures 6 and 7 reveal that the first observed transient (the 0.4 ps spectrum in Figure 7) has a spectrum that extends across the displayed spectral region, with the ground-state bleaching peaks superimposed thereon.

The minima at 545 and 585 nm (Figure 7) correspond to the two Q bands of the ground state. Clearly at 585 nm the extinction coefficient of the removed ground state is greater than that of the formed transient species, hence an overall negative absorbance. This is not so for the 545 nm peak. There is an isosbestic point at 569 nm. Mentally correcting the 0.4 ps spectrum for the ground state absorption loss, it would seem that the first-observed absorption is a continuum across the visible region, with a single peak below 500 nm. Moreover, it is a presumed continuation of the FOT seen as the red curve in Figure 5, generated by the 582 nm excitation.

(b) Dynamic Properties. In Figures 5 and 7, the FOTs are formed in less than the elapsed time of 300 fs, close to the 10−90% rise time of the spectrometer, and it is concluded

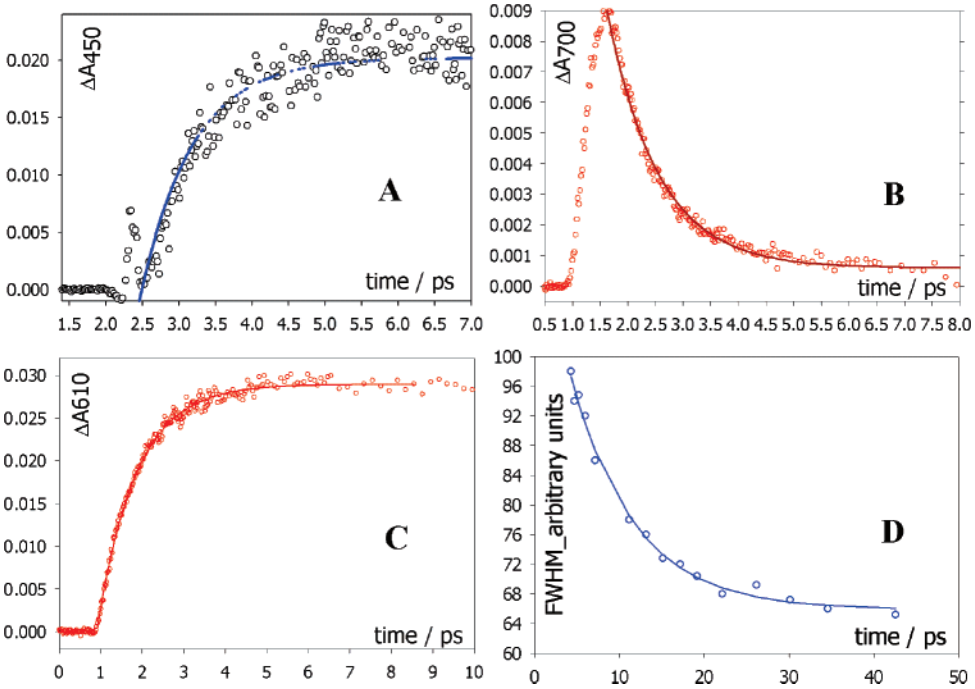

Figure 9. Panels A, B, and C show temporal slices from the surface in Figure 6 at the indicated wavelengths. Panel D shows the temporal progress of the fwhm of the negative absorption band shown in Figure 8.

that the whole of the 400 to >760 nm transient absorption displayed in Figures 5, 6, and 7 increases within our instrument response function. Note that, at the 400 nm excitation, the B state is being pumped and, at 582 nm, the Q state is being generated. Thus, in the case of the 400 nm excitation, the FOT is not identical to the primary state being generated because this is B. The anticipation is that the FOT at both excitation wavelengths is, in fact, the Q state which has been reached by very rapid internal conversion within the instrument response time.

Figure 9A shows that the 450 nm transient is generated from the FOT with a growth lifetime of 710 ± 105 fs. In the orange-red spectral region, the time profile at 700 nm (Figure 9B) shows a rapid rise followed by a decay (decay lifetime = 870 ± 95 fs) and at 610 nm (Figure 9C) the signal grows post pulse (growth lifetime = 980 ± 120 fs). Note that the decay profile at 700 nm is not purely monoexponential; there is a minor (<10%) component with a lifetime of 8.5 ± 0.9 ps. Figures 5 and 7 show that, having been formed, the 450 and 610 nm absorptions become blue-shifted and narrower. The time profile in Figure 9D indicates that the fwhm of the spectral band at 610 nm (nominal) shows an exponential change with a time constant of 7.2 ± 1.0 ps. After ca. 35 ps (Figure 9D), no further spectral narrowing/shifting occurs and the signal decays (Figure 10, upper panel). The initial ca. 20% of the signal had a decay lifetime of 25 ± 1.6 ps, and the remaining 80% had a lifetime of 342 ± 28 ps. This latter process is the one that repopulates the ground state. Indeed, the time profile at 585 nm has the minimum bleaching signal recovered in a biexponential manner with lifetimes of 29.5 ± 3.5 ps (18%) and 305 ± 25 ps (82%) (Figure 10, lower panel). Similar biphasic kinetics were found on the red side of 610 nm, with the faster component showing a wavelength-dependent lifetime (Table 8).

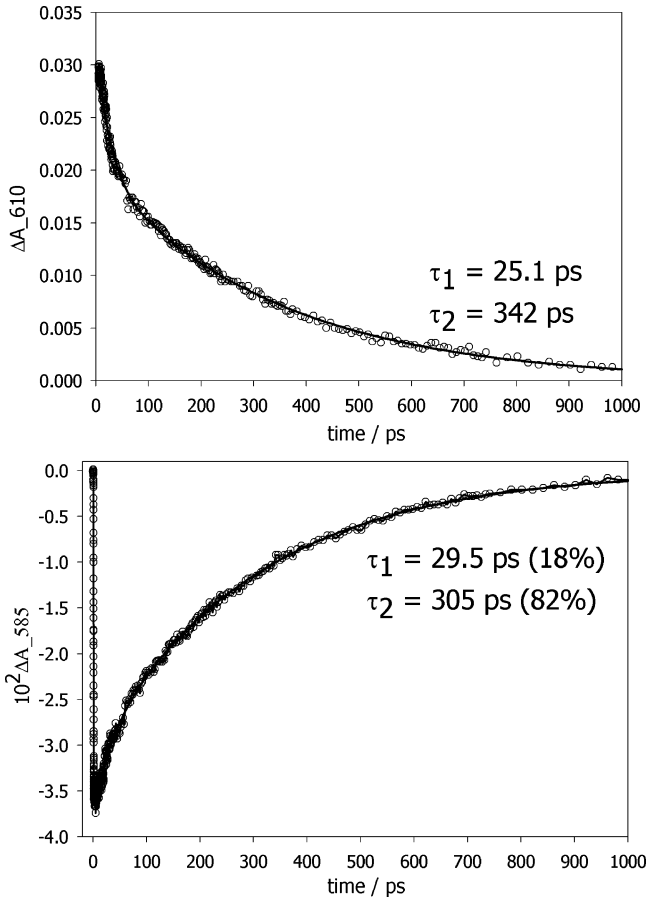

Figure 10. Upper and lower panels show temporal slices from the surface displayed in Figure 6 at the indicated wavelengths. The profiles have been fitted with a sum of two exponentials, see text.

Table 8. Wavelength-Dependent Lifetimes of the Faster Component

wavelength (nm)	τ_1 (ps)	τ_2 (ps)
610	25.1 ± 1.6	342 ± 28
630	7.7 ± 1.0	417 ± 35
640	1.8 ± 0.3	*a*
650	0.98 ± 0.15	*a*

[a] Signal too noisy to obtain a precise lifetime value.

(c) Interpretation of the Photophysical Behavior. Scrutiny of Figures 5, 6, and 7 shows that the FOT, generated during the instrument response time (ca 300 fs), has a positive absorption feature that extends from ca. 420 nm to beyond 700 nm. Superimposed on this are negative peaks near 425, 540, and 585 nm that correspond to the wavelengths at which the ground-state absorption exhibits maxima. Clearly these features are the result of the depletion of ground state concentration by the excitation event, and the negative absorption results from the fact that in these spectral regions the extinction coefficient of the lost ground state exceeds that of the produced FOT. There is no discernible difference between the spectral features of the FOT at either of the excitation wavelengths, allowing the conclusion that the FOT is the Q state that is pumped directly by the 582 nm radiation and is formed within the instrument response time after pumping with 400 nm radiation. Figure 9B shows that the Q state decays to a small nonzero baseline with a lifetime of 870 ± 95 fs. At 450 nm (Figure 9A), the signal grew with a lifetime of 710 ± 105 fs, and at 610 nm (Figure 9C), the signal formation had a 980 ± 120 fs growth lifetime. These three lifetime values are sufficiently close so that it can be concluded that the Q state has a decay lifetime of 850 ± 110 fs and is the precursor of a transient species which has absorption bands near 450 and 600 nm. As Figures 5, 7, and 8 show, the spectrum of this daughter species narrows and blue shifts; the clearest indication of this is in Figure 8. The fwhm of the negative band near 585 shows an exponential shift with a 7.2 ps lifetime. Moreover, as can be seen in Table 8, the second species decays in a biphasic manner according to the sum of two exponentials, the first of which shows a wavelength-dependent lifetime. This blue shifting and the wavelength-dependent kinetics point to vibrational cooling of the state. As can be seen from Table 8, the lifetime of the faster decay component is significantly longer at the higher-energy spectral region. The vibrationally excited species that appear at the higher spectral energies contain less vibrational energy than those at the red edge of the band because, for $\Delta v = 0$, the transitions between S_0 and S_1 (Q), the transition energies will decrease as v increases. The higher-energy modes have a greater density of acceptor oscillators available for transfer to than the lower-energy modes, and the deactivation rates will be correspondingly more effective and therefore faster. At the end of the cooling phase (and indeed during it), the spectral features in the yellow-green and the red are characteristic of a (d,d) state in which the electronic excitation, initially resident on the π-electronic system has migrated to the metal center causing a change in the d-electron configuration and enhanced nuclear motions. This leaves the π system in its electronic ground state, so that the resulting molecule has an absorption spectrum that is dominated by the (π,π*) transitions (i.e., similar to the initial ground-state spectrum with a spectral shift that is a consequence of the different d-electron configurations). It is important to note that in NiOMTP this shift is to the red, as has been reported for planar nickel porphyrins such as NiOEP, NiTPP, and NiPPDME (PPDME = protoporphyrin(IX) dimethyl ester).[28]

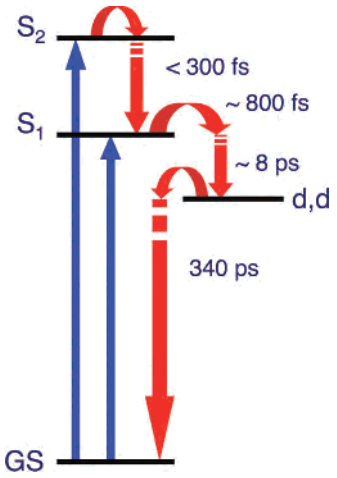

Figure 11. Proposed deactivation scheme for the S_1 and S_2 states of NiOMTP.

Table 9. Excitation Energies (eV), Composition, and Character of the Excited States of NiOMTP Lying Below the S_1 (π,π*)

state	composition (%)	character	E_{va}	E_{adia}
2^3A_2	96 ($26b_2 \rightarrow 23b_1$)	LMCT	2.01	
1^1B_2	100 ($47e \rightarrow 48e$)	MLCT	1.94	
2^1A_1	75 ($22b_1 \rightarrow 23b_1$)	LMCT	1.94	
2^3A_1	97 ($22b_1 \rightarrow 23b_1$)	LMCT	1.89	
1^1B_1	96 ($47e \rightarrow 48e$)	MLCT	1.88	
1^1A_2	99 ($47e \rightarrow 48e$)	MLCT	1.87	
4^3E	96 ($26b_2 \rightarrow 48e$)	π,π*	1.87	
1^1E	99 ($28a_1 \rightarrow 48e$)	MLCT	1.83	
3^3E	97 ($22b_1 \rightarrow 48e$)	π,π*	1.81	
1^3A_2	100 ($47e \rightarrow 48e$)	MLCT	1.79	
2^3B_1	100 ($47e \rightarrow 48e$)	MLCT	1.78	
2^3E	99 ($28a_1 \rightarrow 48e$)	MLCT	1.78	
1^3B_2	100 ($47e \rightarrow 48e$)	MLCT	1.75	
1^3A_1	97 ($47e \rightarrow 48e$)	MLCT	1.73	
1^3E	96 ($47e \rightarrow 23b_1$)	d_π,$d_{x^2-y^2}$	1.57	1.09 (1^3B_3)[a]
1^3B_1	100 ($28a_1 \rightarrow 23b_1$)	d_{z^2},$d_{x^2-y^2}$	1.42	0.88[b]

[a] The energy value refers to the Jahn−Teller distorted D_2 structure. [b] The energy value refers to the structure optimized under the D_{2d} symmetry constraint.

Taken together, the spectral and dynamics results provide evidence that the Q state reaches the initial ground state by way of an electronically excited metal-centered state (Figure 11).

(d) Deactivation of the S_1 (Q) State: Insights from Theory. To gain an insight into the deactivation mechanism of the S_1 (Q) state, we have examined the lowest singlet and triplet excited states of NiOMTP. The vertical absorption energies calculated for the whole set of singlet and triplet states lying below the S_1 (Q) state are gathered in Table 9.

The TDDFT results locate five singlet and two triplet excited states between the S_1 (Q) state and the lowest triplet (π,π*), the 3^3E, which is the emissive $^3T_1$ in luminescent metalloporphyrins. Except for the higher lying triplet (π,π*), the 4^3E, the one often referred to as $^3T_2$, these states have

LMCT (2^3A_2, $2^{1,3}A_1$) or MLCT character (1^1B_2, 1^1B_1, 1^1A_2, 1^1E). A manifold of triplet states is found to lie vertically below the $^3T_1$ (Table 9). Five of these have MLCT character, while the lowest two, (1^3E and 1^3B_1) have d,d character, being described by the 47e $\rightarrow$ $23b_1$ ($d_\pi \rightarrow d_{x^2-y^2}$) and $28a_1$ $\rightarrow$ $23b_1$ ($d_{z^2} \rightarrow d_{x^2-y^2}$) transitions, respectively. These appear vertically at 1.57 (1^3E) and 1.42 eV (1^3B_1). Their corresponding singlets, the 3^1E and 3^1B_1, both lie above the S_1 (Q) state, at 2.15 and 2.47 eV, respectively, and cannot play a role in the deactivation of the Q state. The large singlet/triplet splitting computed for these (d,d) states fits in with the high localization of the unpaired electrons on the metal center. The $^1B_1/^3B_1$ splitting is larger than the $^1E/^3E$ splitting (1.05 vs 0.58 eV) because of the more pronounced d,d character of the associated one-electron transitions (cf. the MO compositions in Table 3).

On the basis of the vertical absorption energies, the transient species responsible for the derivative-shaped spectrum (Figures 5 and 7) could be assigned to either the 1^3B_1 (d,d) state or the 1^3E (d,d) which lies only 0.15 eV vertically above the 1^3B_1. To elucidate this question, we considered the effect of geometrical relaxation. The computed values of E_{adia} shown in Table 9 indicate that after the inclusion of geometrical relaxation the relative ordering of these states is retained.

As can be inferred from Table 9, the adiabatic energies of the 1^3B_1 and 1^3E states are both significantly decreased by $\sim$0.5 eV relative to the corresponding vertical absorption energies. This fits in with the relaxed geometry of these states (note that the doubly degenerate 1^3E state Jahn$-$Teller distorts into a D_2 structure) showing significant changes with respect to the ground-state geometry, as can be seen in Table S2, which collects the optimized geometries of the 1^3B_1 and 1^3E states. In both cases, the relaxed geometry is characterized by a considerable lengthening of the Ni$-$N distance, a sizable expansion of the macrocycle core, and a reduced ruffling distortion ($\sim$75%). These geometrical changes are directly related to occupation of the $23b_1$, a strongly σ antibonding Ni$-$N orbital (see plot in Figure 3). We note that, similar to the ^{3}(d,d) states, the LMCT states in the upper reaches of the manifold (i.e., the 2^3A_2, $2^{1,3}A_1$), which all involve population of the $23b_1$ orbital, are also expected to undergo a large geometrical relaxation. Their relaxed energy surfaces might even cross the surfaces of the ^{3}(d,d) states, but it is very unlikely that the minima of their relaxed energy surfaces will end up below that of the 1^3B_1. Thus, we may conclude that the 1^3B_1 is the lowest intervening state prior to the ground state, and hence, the experimentally observed derivative spectra (Figures 5 and 7) can be assigned to this state. The abundance of states lying between the Q state and the 1^3B_1 (Table 9) well accounts for the experimentally observed fast decay of the S_1 to the 1^3B_1 state.

Conclusions

The ground- and excited-state properties of a Ni(II) porphyrin bearing pheripheral methylthio groups, NiOMTP, have been investigated by steady-state and time-resolved spectroscopy and DFT/TDDFT theoretical methods. In the absence of structural data, several conformations corresponding to different deformations of the porphyrin core and to different orientations of the methyllthio groups have been theoretically explored. The nearly degenerate purely ruffled D_{2d} and hybrid (ruffled with some saddling) D_2 conformations, with an up$-$down orientation of the vicinal methylthio groups are found to be the preferred conformations in the "gas phase". It is the orientation of the vicinal methylthio groups rather than the type and degree of distortions of the porphyrin core that determines the stability of the NiOMTP conformers.

The ground-state electronic absorption spectra of NiOMTP show significant differences with the parent NiP and β-alkylated porphyrins such as NiOEP. The most prominent changes consist of (i) a considerable red shift of the B and Q bands, (ii) an intensification and broadening of the Q band, and (iii) additional weak absorptions in the region between the Q and B bands. These changes have been explained in terms of the electronic effects of the methylthio groups, the ruffling of the porphyrin core playing a very minor role. Two electronic structure features are key to an understanding of the observed spectral characteristics. (1) A strong interaction of the π system of the porphyrin ring with the sulfur lone pairs leads to an upshift of the G a_{1u} orbital and, hence, to a significant splitting of the occupied pair of a_{2u}/a_{1u} Gouterman orbitals. The diminished G a_{1u}/G e_g* gap and the lifting of the a_{2u}/a_{1u} degeneracy explain the red shift of the Q and B bands and the hyperchromicity of the Q-band in the complex. (2) The methylthio groups introduce additional levels with sulfur lone pair character in the valence region. According to the ultrafast transient absorption measurements performed in toluene and the TDDFT calculations of the lowest-excited states, the Q state of NiOMTP deactivates by the pathway $^1(\pi,\pi^*) \rightarrow {}^3(d_{z^2},d_{x^2-y^2}) \rightarrow$ ground state. The (d,d) state exhibits complex spectral evolution over ca. 8 ps, interpreted in terms of vibrational relaxation and cooling. The cold ligand-field excited state decays with a lifetime of 320 ps. In contrast with the highly distorted nickel porphyrins but similar to the planar analogues, the (d,d) spectrum of NiOMTP has transient absorption bands immediately to the red of the bleaching of the ground-state Q and B bands.

Acknowledgment. The photophysical studies conducted at the Ohio Laboratory for Kinetic Spectrometry (BGSU) were supported in part by NIH Grant CA 91027 and by an instrumentation grant from the Hayes Investment Foundation (Ohio Board of Regents). A.R. and G.R. wish to thank the Italian MIUR (Ministero dell′ Istruzione, dell′ Università e della Ricerca) and the Università della Basilicata, Italy, for a grant (Grant 2003038084_002).

Supporting Information Available: Energies and percentage composition of the highest-occupied and lowest-unoccupied MOs of NiP in the planar (D_{4h}) and ruffled (D_{2d}) conformations (Table S1) and optimized geometrical parameters for the triplet (d,d) excited states of NiOMTP (Table S2). This material is available free of charge via the Internet at http://pubs.acs.org.

IC050838T